Electronic Supplementary Material (ESI) for Journal of Materials Chemistry A.

Supporting information

Unveiling the effect of growth time on the bifunctional layered hydroxide electrodes for high-performance energy storage and green energy conversion

Jyoti Prakash Das[1], Swapnil Shital Nardekar[1], Dhanasekar Kesavan [1], Kousik Bhunia[1]

Ravichandran Vishwanathan[1], Sang-Jae Kim[1,2,3*]

[1]Nanomaterials & System Lab, Major of Mechatronics Engineering, Faculty of Applied Energy System, Jeju National University, Jeju- 63243, Republic of Korea.

[2]Nanomaterials & System Lab, Major of Mechanical System Engineering, College of Engineering, Jeju National University, Jeju- 63243, Republic of Korea.

[3]Research Institute of New Energy Industry (RINEI), Jeju National University, Jeju- 63243, Republic of Korea.

*Corresponding Email id.: kimsangj@jejunu.ac.kr

Materials and methods

S1. Materials

The precursor materials such as Nickel Nitrate hexahydrate ($Ni(NO_3)_2 \cdot 6H_2O$), Cobalt nitrate hexahydrate($Co(NO_3)_2 \cdot 6H_2O$), HMTA, and Potassium hydroxide were procured from Daejung Chemicals & metals co.Ltd., S. Korea. The materials were used for application without any post-treatment in analytical grade without any prior treatment.

S2. Instrumentation

The crystal structure and phases of the NiCo LDH electrode were analyzed using an Empyrean X-ray diffractometer (XRD) (Malvern Pan analytical, UK). The source of the XRD was Cu-Kα under a current of 40mA and a voltage of 40kV. The Laser Raman for the NiCo LDH was carried out using LabRAm HR Evolution Raman Spectroscopy (Horiba Jobin-Yvon, France) with Ar^+ ion laser functioning at 10mW power with the excitation wavelength of 514nm. The morphology of the NiCo LDH was analyzed using a Field emission scanning electron microscope (TESCAN, MIRA3) coupled with an energy-dispersive X-ray spectroscopy (EDS) analyzer for the quantitative analysis of the samples. The electrochemical performance of the active electrode or ASC device was analyzed using an AUTOLAB PGSTAT302N electrochemical workstation. The Brunauer-Emmett-Teller (BET) surface area of composites analyzed based on the des-adsorption isotherms of inert nitrogen was performed using BELSORP MINI X, Microtrac MRB Chem BET analyzer. All samples were degassed under vacuum conditions at 250 ºC for 4 h. The apparent surface area was computed from the nitrogen adsorption data in the relative pressure range between 0.05 and 0.3.

S3. Synthesis of NiCo LDH

NiCo LDH were directly grown over Ni-foam via the one-step hydrothermal process. At first, the precursor solution was prepared by homogeneous mixing of $Ni(NO_3)_2 \cdot 6H_2O$ and $Co(NO_3)_2 \cdot 6H_2O$ with $C_6H_{12}N_4$ in the ratio of 2:1:3 in 40 ml DI water to allow for constant stirring until the formation of a light pink colour solution. Prior to the hydrothermal deposition, We have followed the standard protocol for the mass calculation after the hydrothermal growth of the Ni-Co LDH over the nickel foam. Step 1: The NF substrate is cleaned thoroughly with dilute HCl and ethanol to remove the oxide layer and the volatile substances respectively and kept for drying at 80˚ C for 4 h. After drying the weight of the NF was measured and noted as W1. Step 2: Then the cleaned NF was kept for the hydrothermal reaction for the designated

period and cleaned thoroughly with absolute ethanol and DI water to remove the excess deposits and kept for drying for 6 hours to remove all the moisture contents. After drying the weight of the hydrothermally treated NF with grown NiCo LDH for 3 different time intervals [6h,8h,10h] is measured and the weight is recorded as W2. The difference between W2 and W1 is obtained as the effective mass of the grown NiCo LDH over the NF. After that, as grown Ni-foam was taken out and rinsed several times with ethanol and DI water. At last, Nico LDH@ Ni electrode was dried in a hot air oven (70°C) for overnight and used for further study. The NiCo LDH samples obtained at various reaction time intervals (from 6 to 10 h) were named as NiCo LDH-6, NiCo LDH-8, and NiCo LDH-10, respectively.

S4. Preparation of graphene oxide (GO) and reduced graphene oxide (rGO) nanosheets

The graphene oxide (GO) sheets were prepared using the modified Hummers' method, whereas the reduced graphene oxide (rGO) sheets were prepared via a thermal reduction method, as reported in the literature[1,2].

S4. Electrochemical analysis of active electrodes via three-electrode configuration

The electrochemical characterizations of as properad electrodes were carried out in three-electrode (3E) configuration method by employing NiCo LDH or graphene as the working electrode, platinum sheet as the counter electrode, and Ag/AgCl as the reference electrode with 3M KOH solution as the electrolyte at room temperature. Here, the active mass loading of the electrode was measured using the Dual range Semi-micro-Balance (AUW-220D, Shimadzu) from the difference between mass before and after hydrothermal treatment/ slurry coating. The performance evaluation of electrode or ASC device were analysed through the best practice methods such as cyclic voltammetry (CV), galvanostatic charge-discharge (CD) and electrochemical impedance spectroscopy (EIS), respectively.

S4. Electrochemical studies of NiCo LDH//Graphene ASC device via two-electrode configuration

The asymmetric supercapacitor was fabricated by sandwiching positrode (NiCo LDH) and negatrode (rGO) having cross-sections (1*1) cm^2 separated by a whatmann paper as a separator and tied together with Teflon tape. The as-prepared device was dipped in a cylindrical beaker in a 3M KOH electrolyte solution. The charge balancing of both (positrode and negatrode) electrodes was done by using following equation as suggested in the previous literature [34].

$m^+ / m^- = [C^- \times \Delta V^-] / [C^+ \times \Delta V^+]$…… (1)

where m^- and m^+ represent the mass of the negative and positive electrodes, C^- and C^+ denote the specific capacitance of the negative and positive electrodes, and, ΔV^- and ΔV^+ are the potential window of the negatrode and positrode obtained using the three-electrode system, respectively. The active mass of the positive and negative electrodes are 0.95 mg and 2.33 mg. The mass of the device is 3.28 mg. The specific capacitance (C_{sp}), specific capacity (Q), energy density (E), and power density (P) of the fabricated asymmetric supercapacitor were calculated using the following equations [5–7].

$$C_{sp} = \int I\, dV / \Delta V * M * S \text{----------(1)}$$

$$C_{sp} = I \times \Delta t / \Delta V \times M \text{----------(2)}$$

$$Q = [I \times \Delta T] / [m*3.6] \text{----------(3)}$$

$$E = (C_{sp} \times \Delta V^2)/2 \text{----------(4)}$$

$$P = E / \Delta t \text{----------(5)}$$

Here "C_{sp}" and "Q" are the specific capacitance (Fg^{-1}) and capacity (mAh g^{-1}); "I" is the current "Δt" is the discharge current(s), "ΔV" is the operating potential window (V); "M" is the mass of the electrode (g), "E" is the energy density and "P" is the power density respectively [8–12].

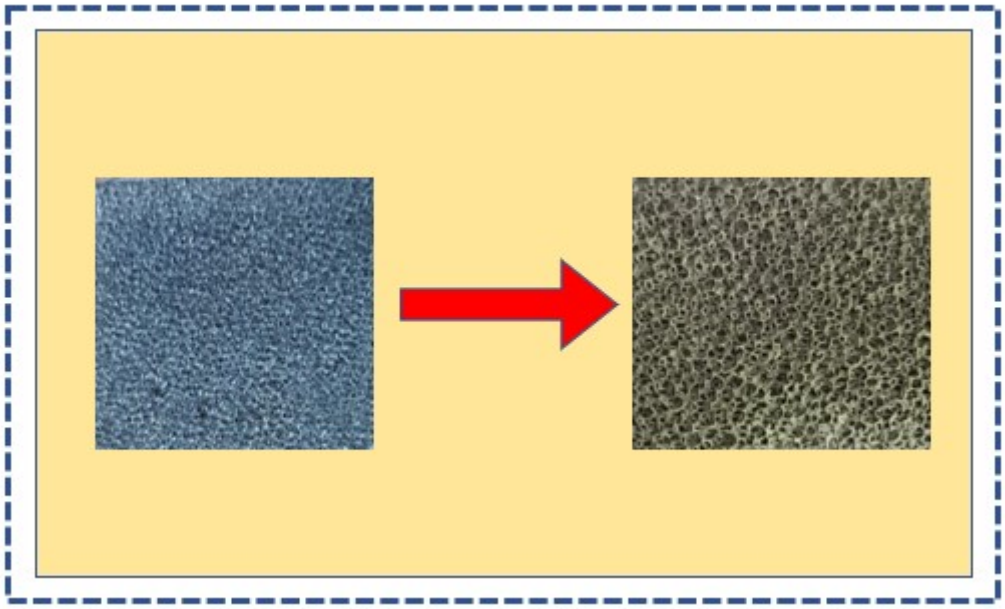

Figure S1. Growth of NiCo LDH over Ni-foam after hydrothermal reaction (10 h).

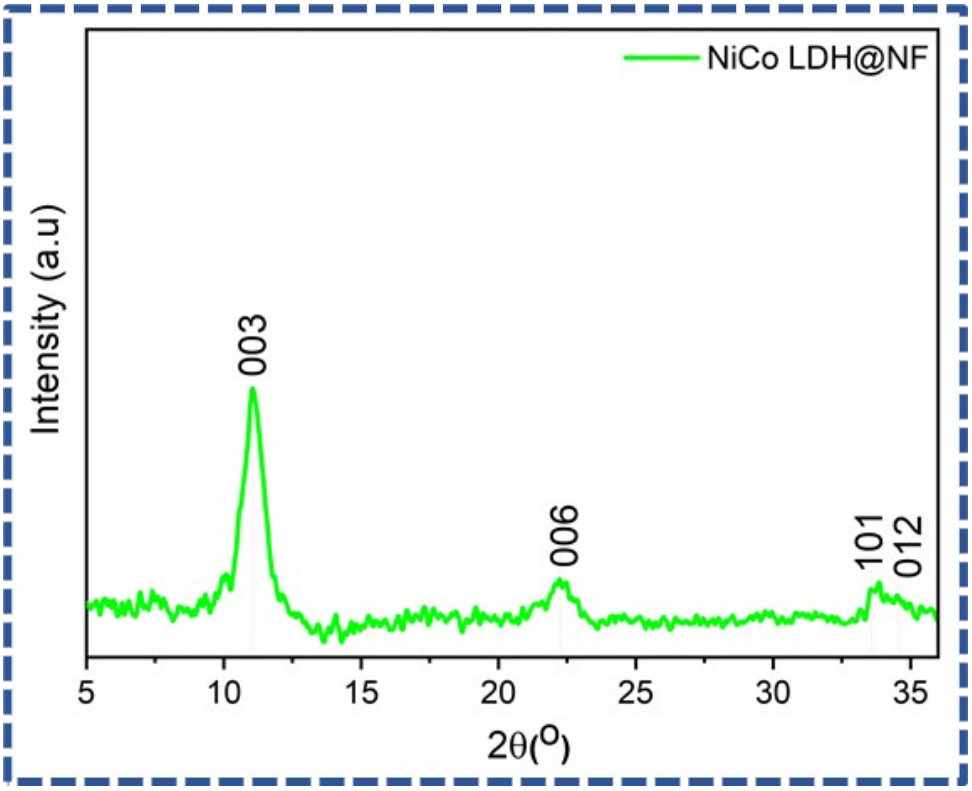

Figure S2.X-ray diffraction pattern of NiCo LDH grown on Ni-foam

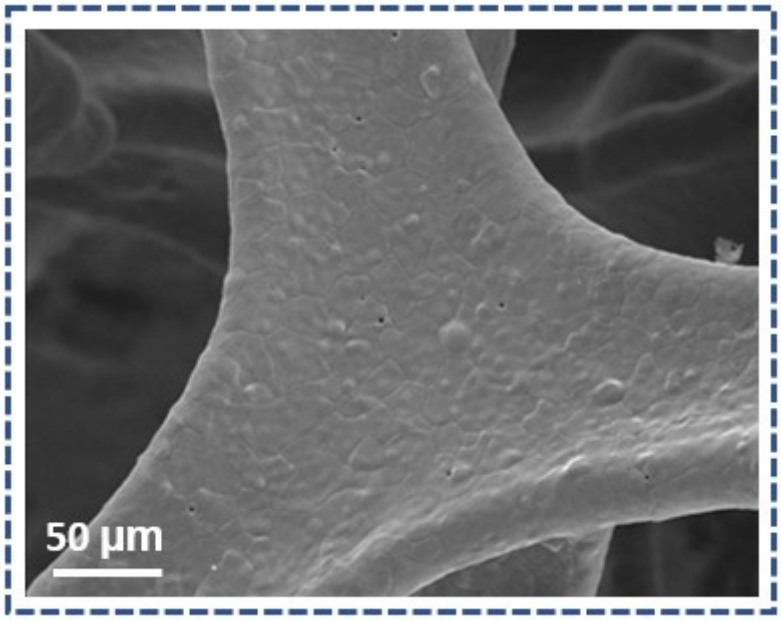

Figure S3. FE-SEM micrograph of bare Ni-foam

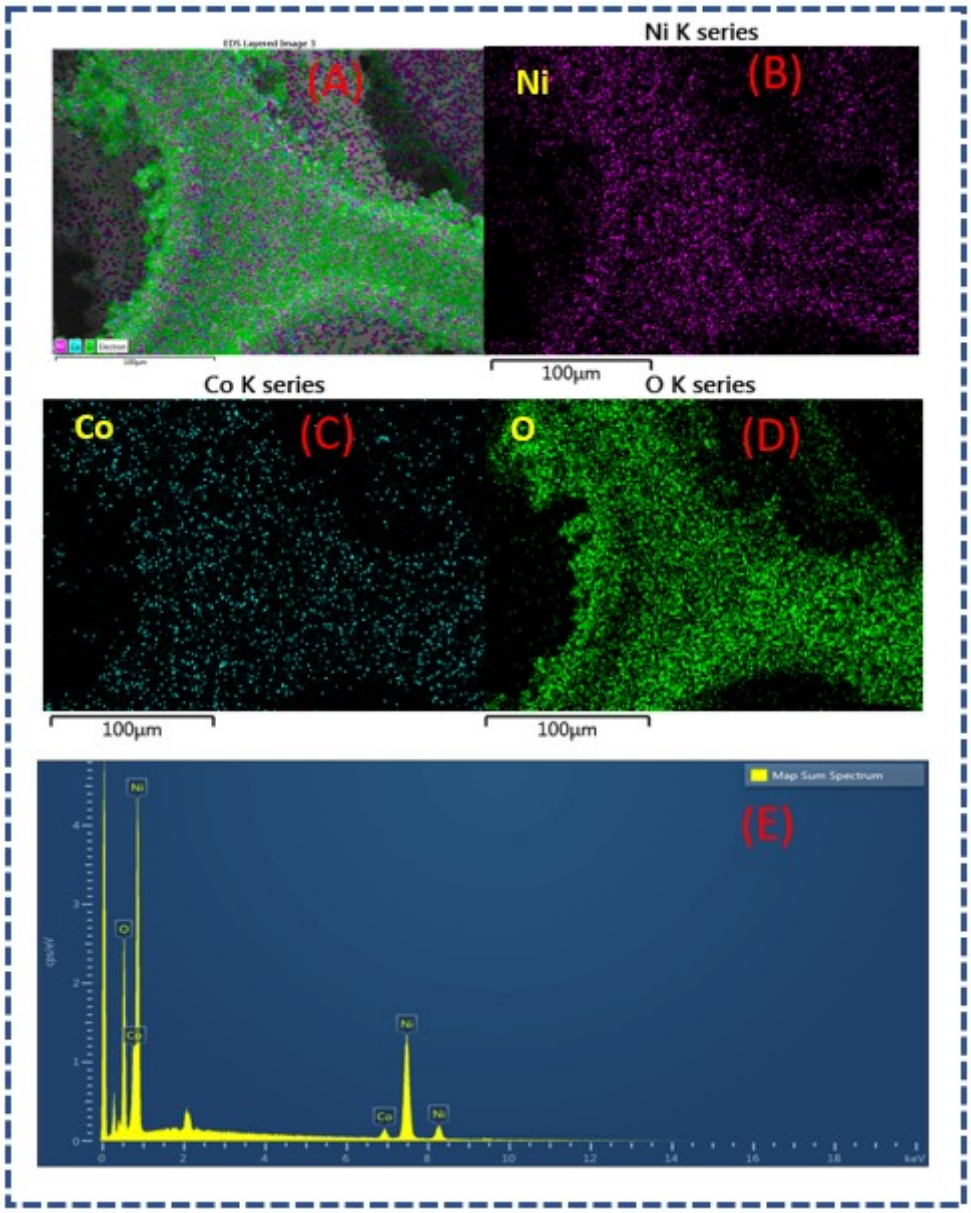

Figure S4. The EDAX mapping depicted the homogeneous growth of Ni, CO, and O homogeneously distributed throughout the Ni-foam (A-E).

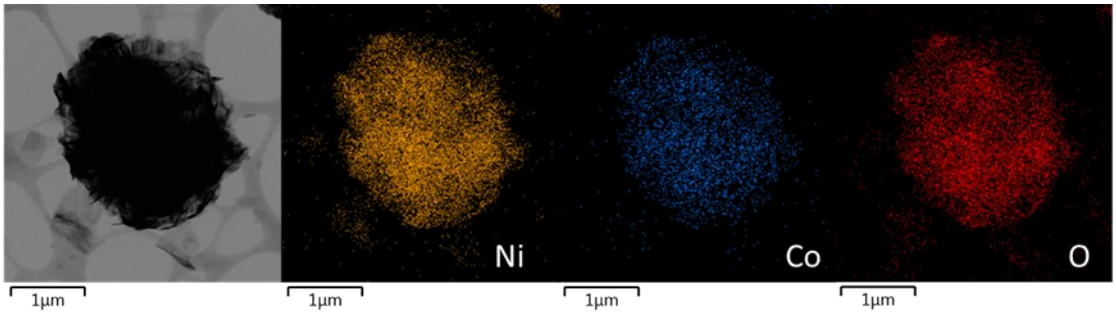

Figure S5 The EDAX mapping confirms the homogeneous distribution of

Ni, CO, and O

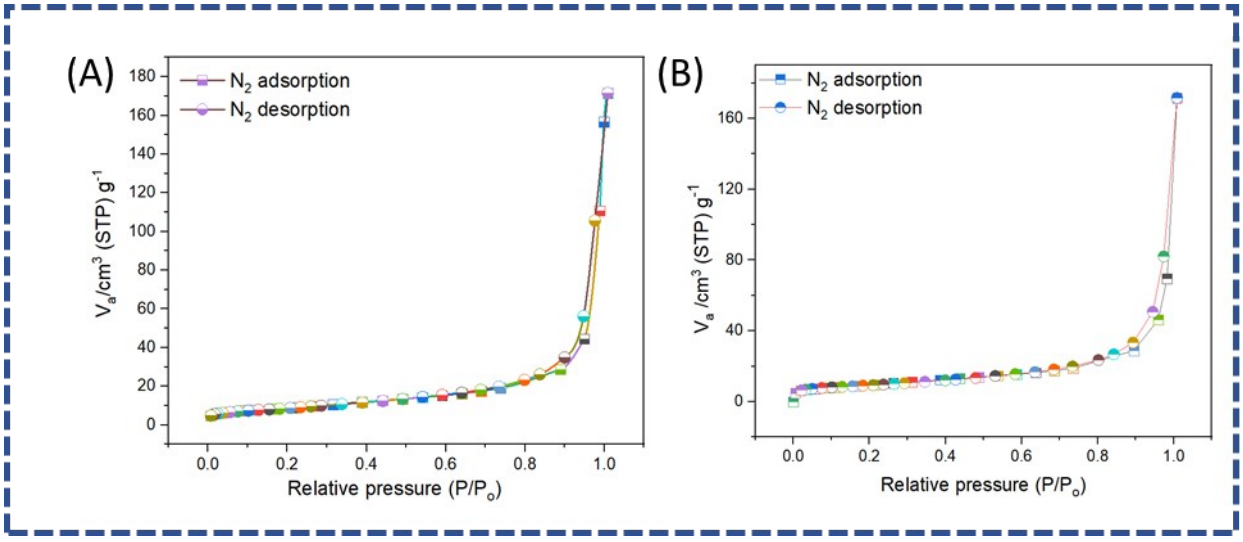

Figure S6.BET surface area analysis (A) NiCo LDH-8 (B) NiCo LDH-6

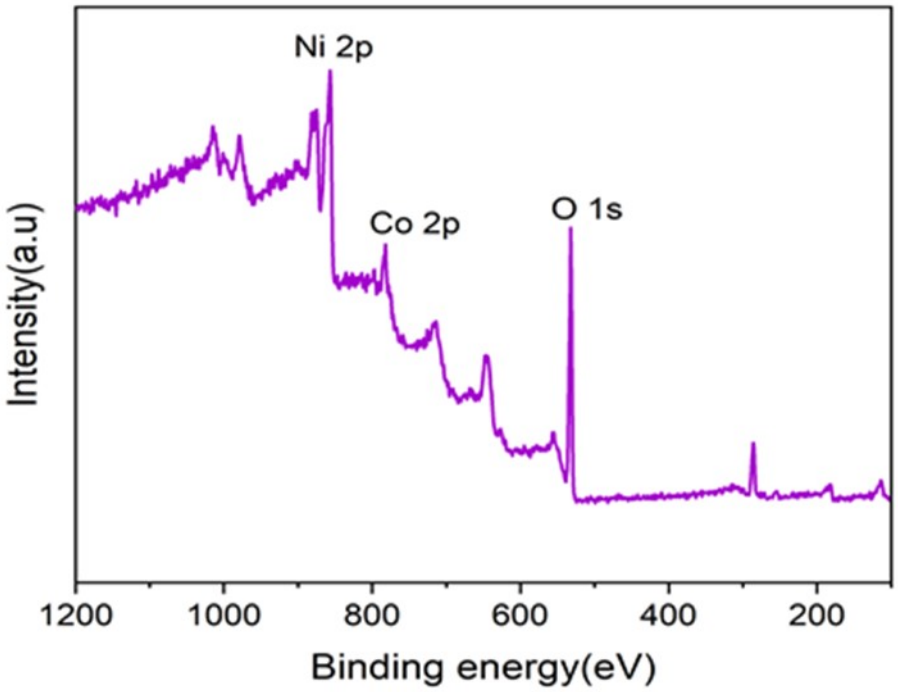

Figure S7.Survey spectrum of NiCo LDH-10

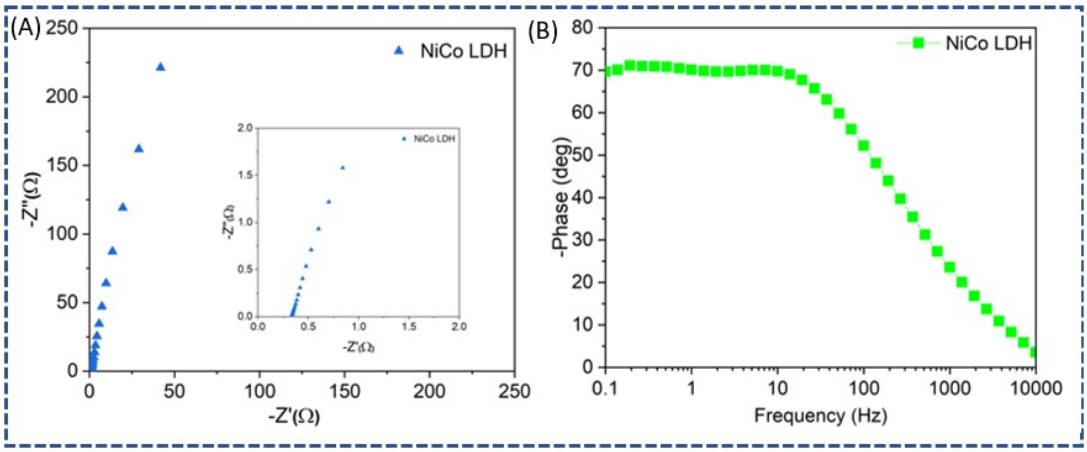

Figure S8. Electrochemical impedance spectroscopy (EIS) analysis of NiCo LDH-10 (A) Nyquist plot (B) Bode phase angle

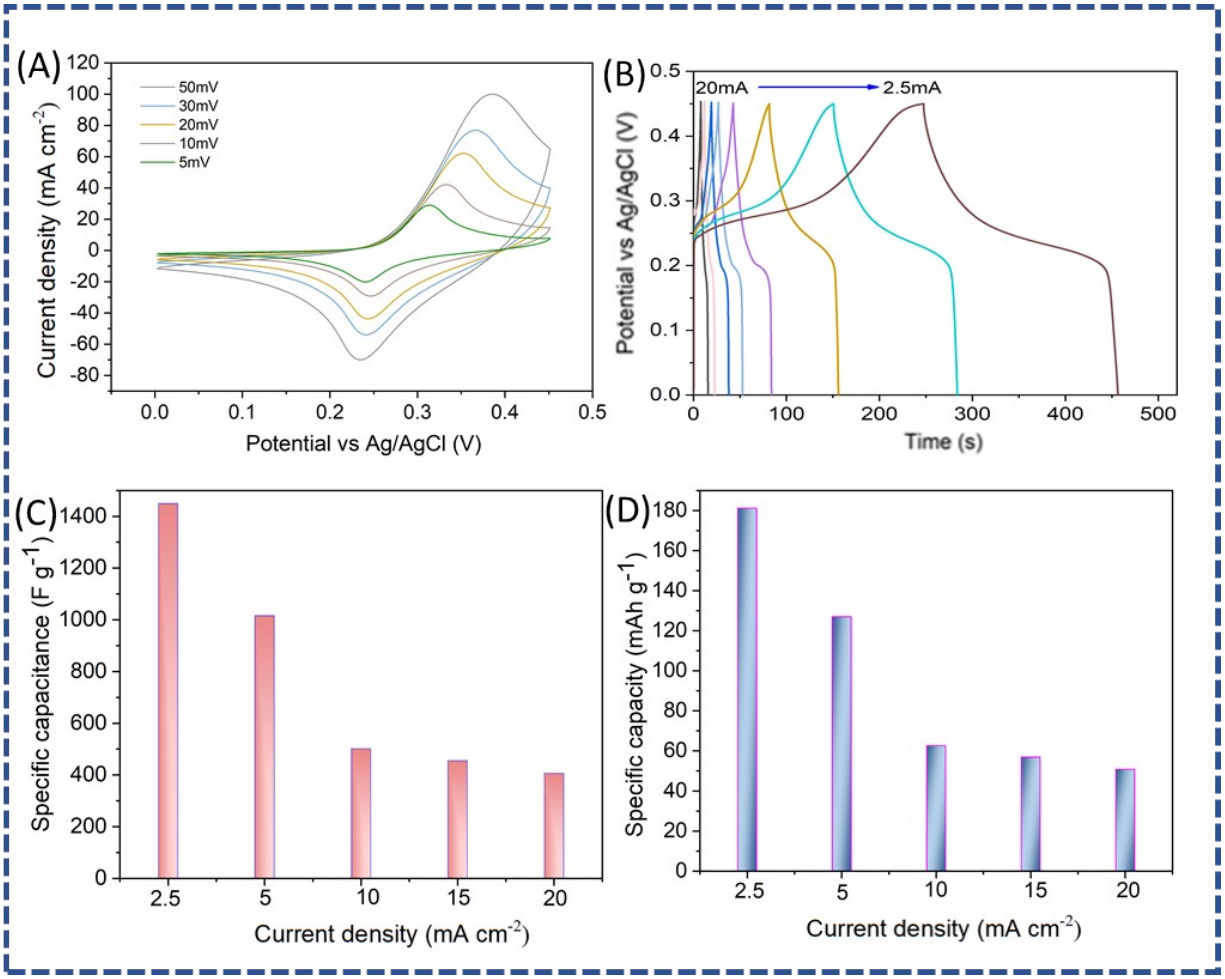

Figure S9. Electrochemical characterization of NiCo LDH-8 (A) Cyclic voltammetry (CV) profiles of NiCo LDH-6 (B) Charge-discharge profile of NiCo LDH electrode measured at various current densities (C) Specific capacitance (D) Specific capacity of the NiCo LDH electrode at various current densities

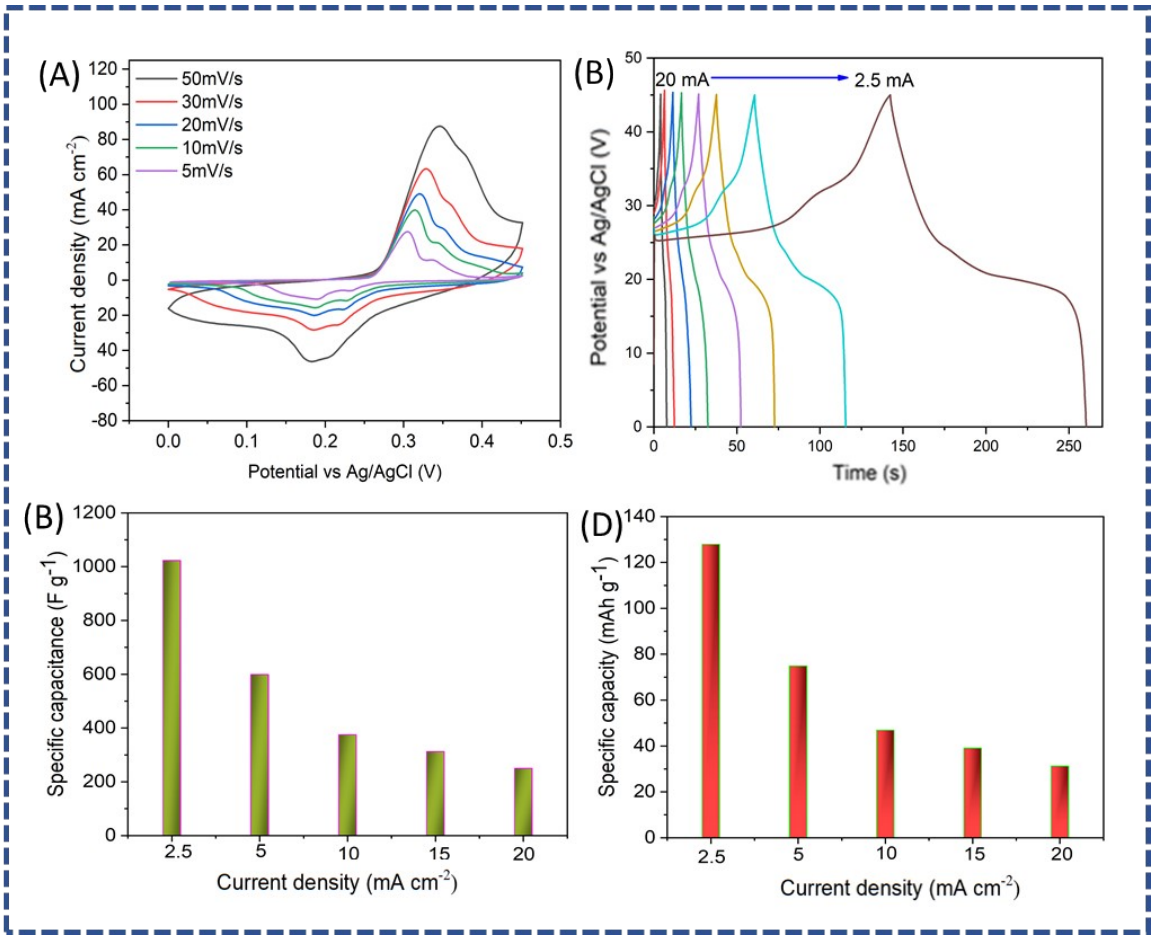

Figure S10. Electrochemical characterization of NiCo LDH-6 (A) Cyclic voltammetry (CV) profiles of NiCo LDH-6 (B) Charge-discharge profile of NiCo LDH electrode measured at various current densities(C) Specific capacitance (D) Specific capacity of the NiCo LDH electrode at various current densities

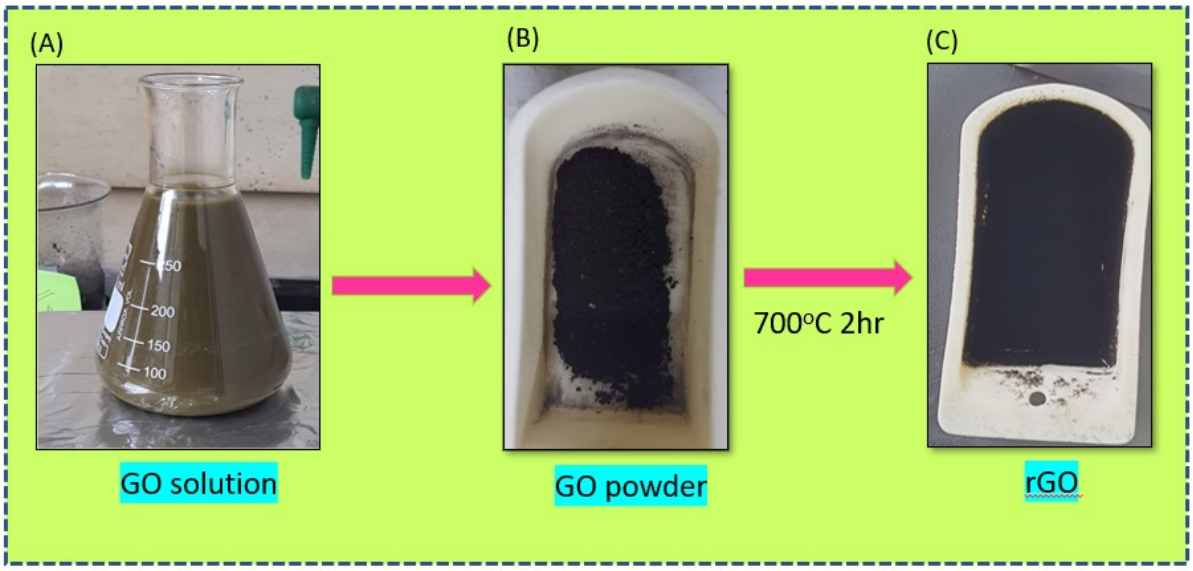

Figure S11. Reduced Graphene oxide (rGO) synthesis (A) Graphene oxide (GO) solution (B) GO powder (C) reduced GO.

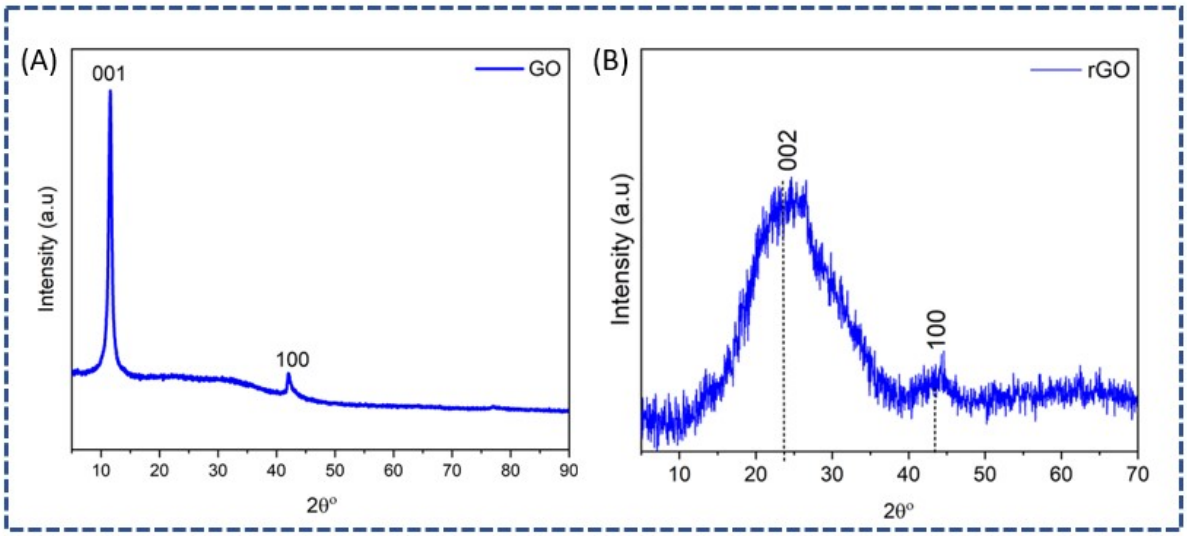

Figure S12. XRD spectra of (A) GO (B) rGO

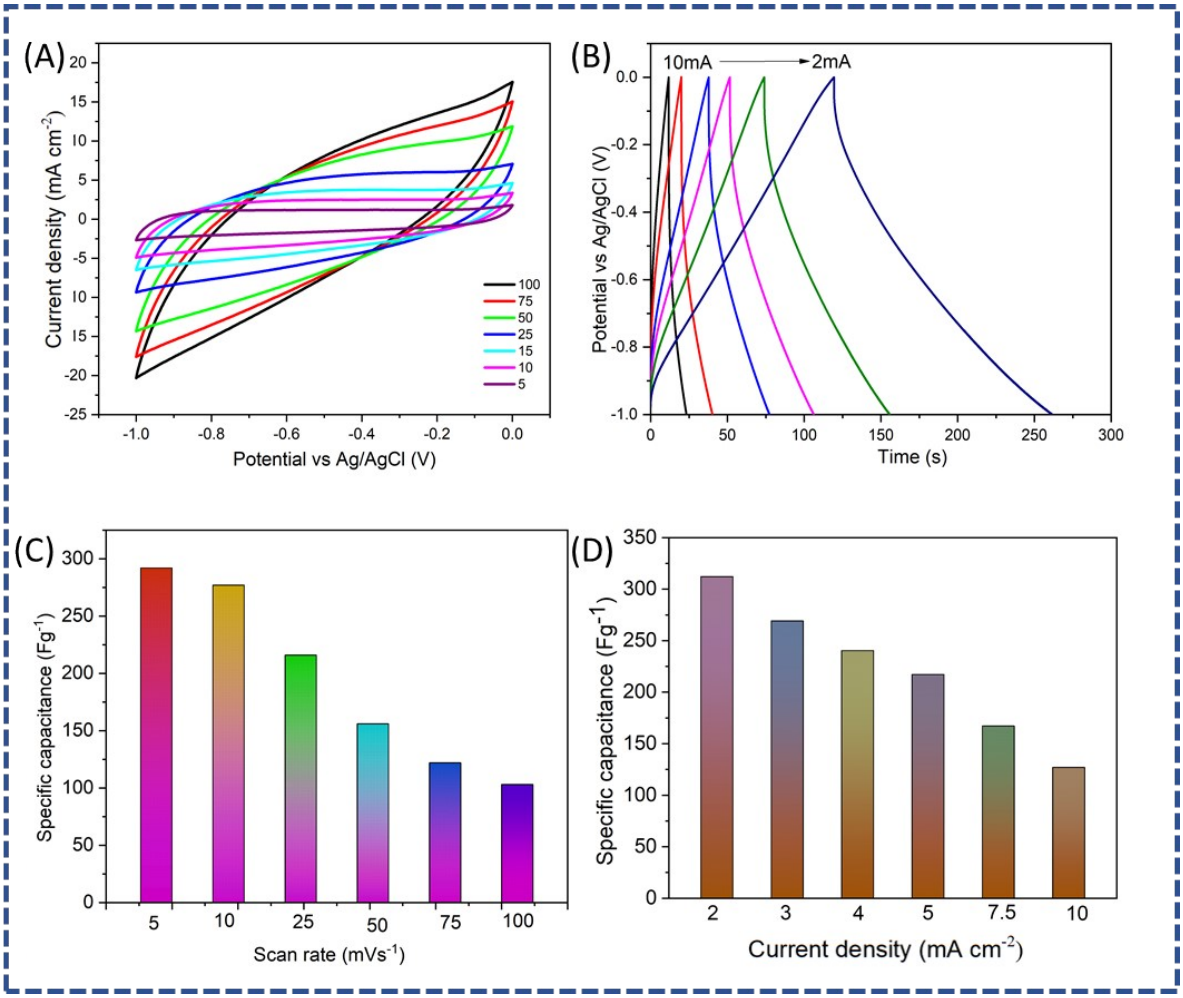

Figure S13. Electrochemical analysis of rGO @NF. (A) Cyclic voltammetry (CV) profiles of rGO@NF (B) Charge-discharge profile of rGO@NF electrode measured at various current densities (C) Specific capacitance from CV (D) Specific capacitance from CD.

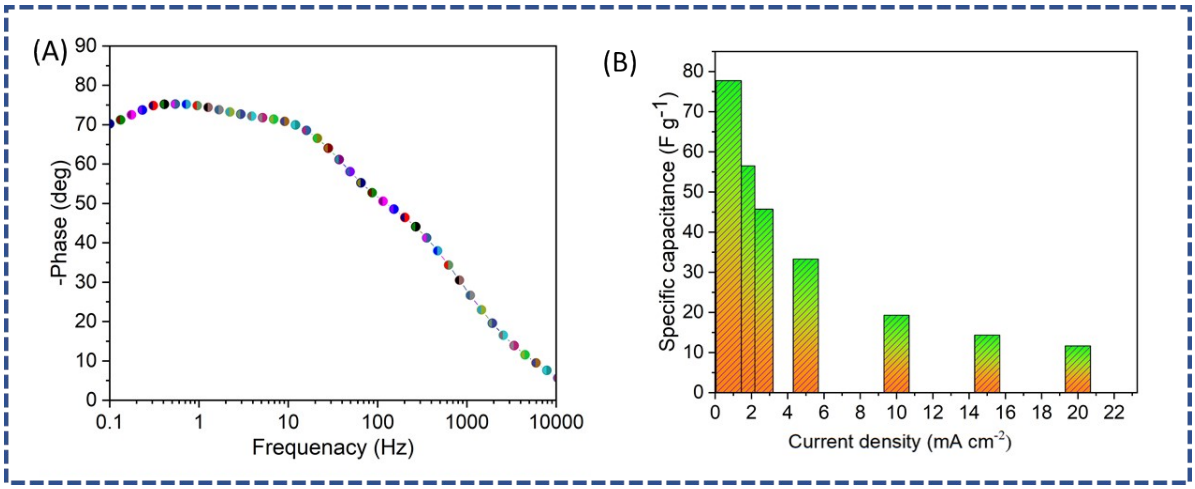

Figure S14. (A) Bode phase angle (B) Specific capacitance of NiCo LDH ‖ rGO ASC device

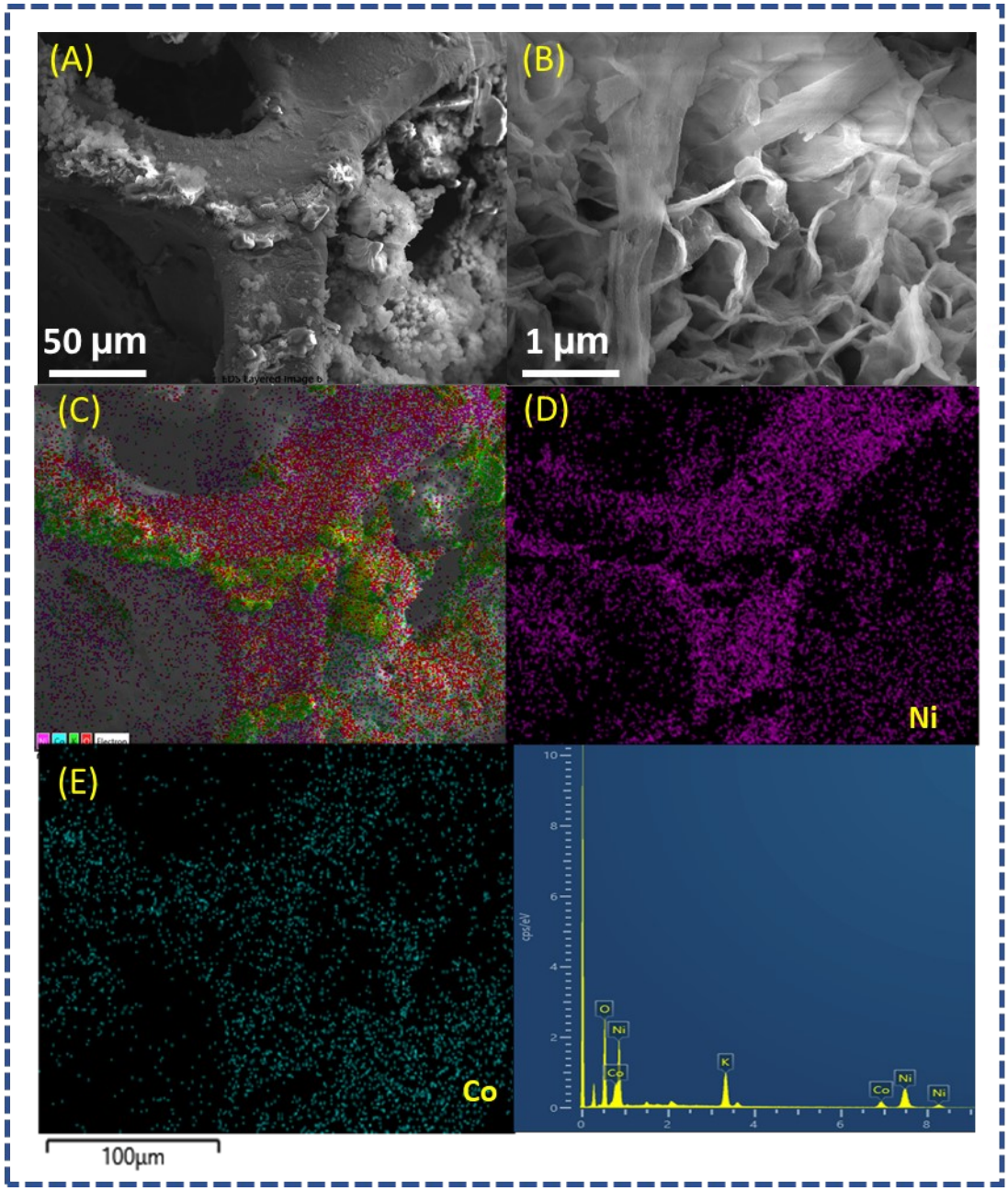

Figure S15. (A-B) SEM micrograph of NiCo LDH electrode after stability study. (C-D) Elemental mapping of Ni, Co over the NF. (F) Map Sum spectrum of NiCo LDH electrode

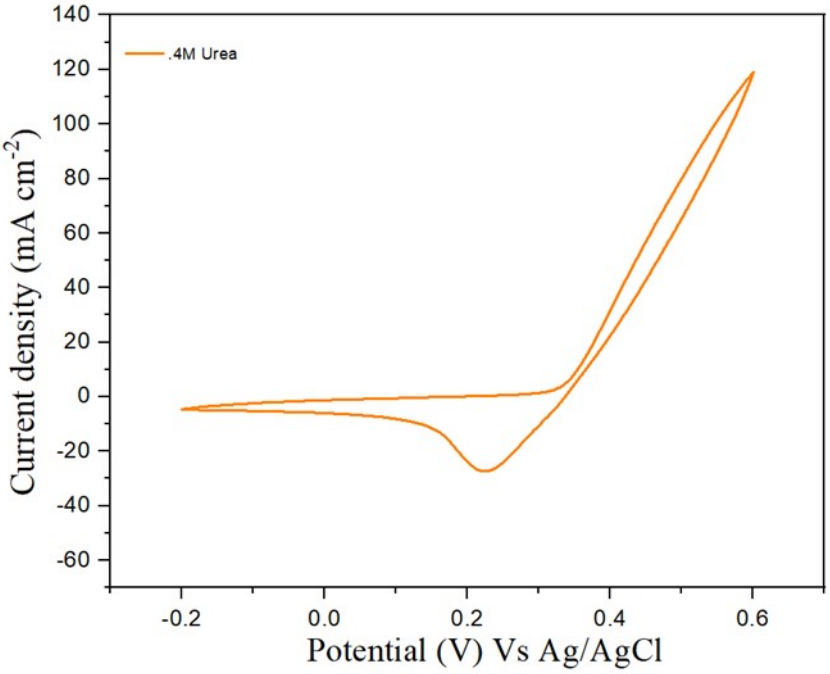

Figure S16. CV curve of NiCo LDH-10 with 0.4 M Urea

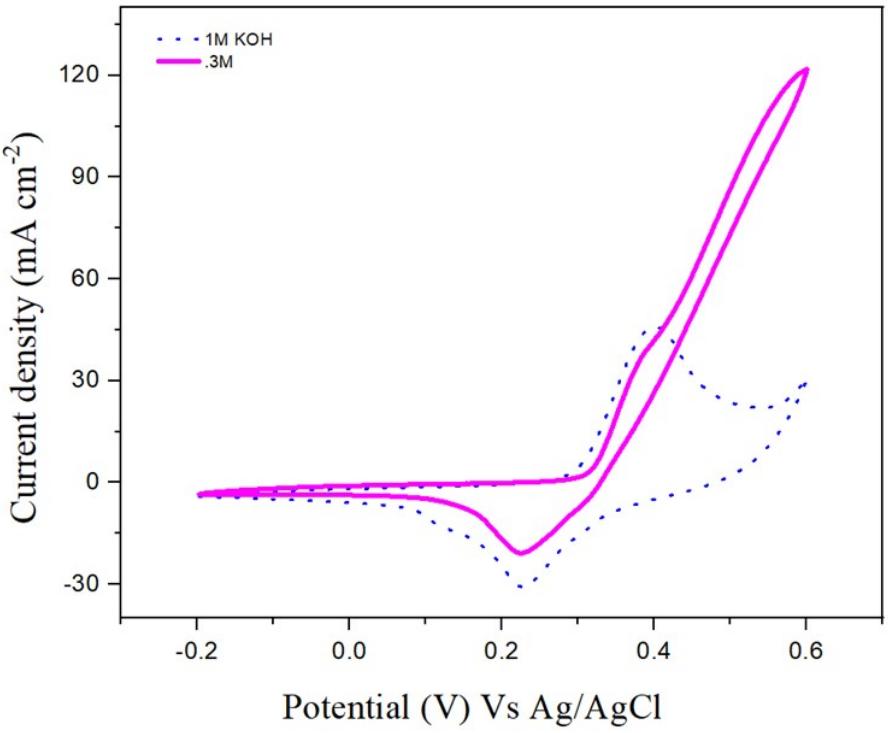

Figure S17. CV curve of NiCo LDH-10 with 3M Urea

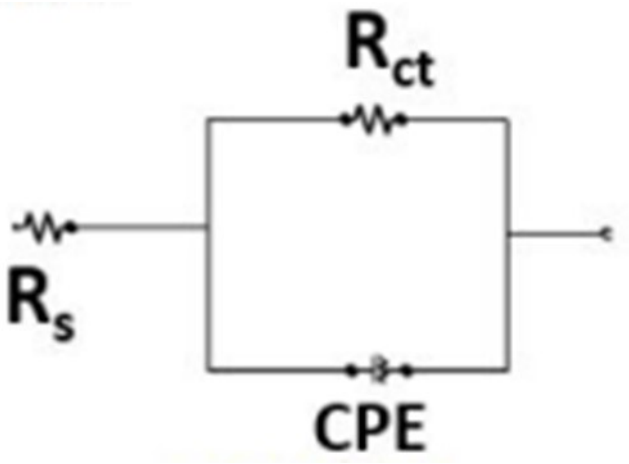

Figure S18. Equivalent circuit diagram

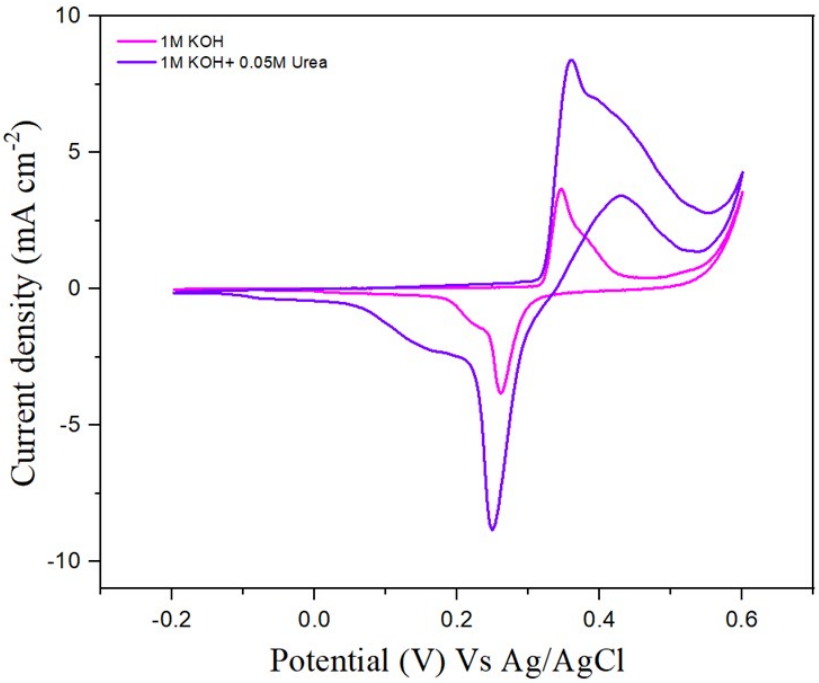

Figure S19. CV curve of bare NF with1M KOH and 0.05M Urea

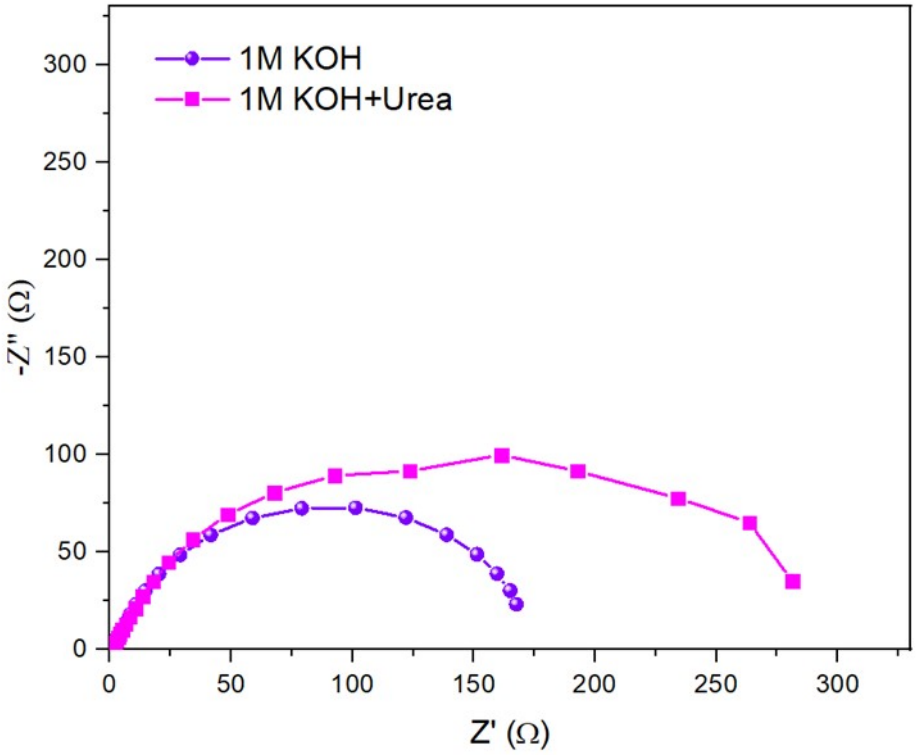

Figure S20. FRA analysis of NF

Materials	Electrolyte	Specific capacitance (F g^{-1})	Cycles	Capacitance retention (%)	Ref.
NiCoMn LDH/rGO	2M KOH	912	5000	63.3%	[13]
NiCoAl-LDH-CNT/RGO	6M KOH	1188	1000	88%	[14,15]
Ni-Co-Mn LDH	2M KOH	2012	1000	57.7%	[15]
Ni0.5Co0.5LDH/AC	1M KOH	947	5000	83.5%	[16]
CoSx/NiCo-LDH	2M KOH	1562	5000	76.62%	[17]
Co-Co LDH/graphene	2M KOH	1205	2000	60.3%	[18]
Ni-Co hydroxides /CNTs	2M KOH	1151	10000	77%	[19]
NiCo-LDH-120/CNTs	2M KOH	1505.4	2000	72.4%	[20]
NiCo LDH/rGO	**3M KOH**	**1684.21**	**5000**	**83.33%**	**This Work**

Table S1. Comparison of specific capacitance of other binder-free NiCo LDH work

Material	Energy density (Wh kg^{-1})	Power density (W kg^{-1})	Ref.
NiFe-LDH@CoS_2@Ni//AC	15.84	375.1	21
Co-Fe LDH@NiO-Ni//AC	22	800	22
NiFe-LDH@MnO_2//NiFe-LDH@FeOOH	22.68	750	23
NiCoFe-LDH//AC	8.7	62.8	24
$NiCo_2S_4$/CFP//AC	17.3	180	25
$NiCo_2S_4$/GA//AC	20.9	800	26
$NiCo_2S_4$ @ PANI-5 //AC	18.86	1285.9	27
GRH-$NiCo_2S_4$//AC	19	703	28
4M-P@NiCo LDH//AC	18.1	750	29
NiCo LDH//rGO	**22.6**	**169.9**	**This Work**

Table S2. Energy density vs Power density of various binder-free NiCo LDH works.

References:

1. Saleem, H., Haneef, M. & Abbasi, H. Y. Synthesis route of reduced graphene oxide via thermal reduction of chemically exfoliated graphene oxide. *Mater Chem Phys* **204**, 1–7 (2018).

2. Oliveira, A. E. F., Braga, G. B., Tarley, C. R. T. & Pereira, A. C. Thermally reduced graphene oxide: synthesis, studies and characterization. *J Mater Sci* **53**, 12005–12015 (2018).

3. Nagaraju, G., Sekhar, S. C., Ramulu, B., Arbaz, S. J. & Yu, J. S. Multicomponent architectured battery-type flexible yarns for high-performance wearable supercapatteries. *Chemical Engineering Journal* **411**, 128479 (2021).

4. Pazhamalai, P., Krishnamoorthy, K., Sudhakaran, M. S. P. & Kim, S. J. Fabrication of High-Performance Aqueous Li-Ion Hybrid Capacitor with $LiMn_2O_4$ and Graphene. *ChemElectroChem* **4**, 396–403 (2017).

5. Qin, K. *et al.* Designed synthesis of NiCo-LDH and derived sulfide on heteroatom-doped edge-enriched 3D rivet graphene films for high-performance asymmetric supercapacitor and efficient OER. *J Mater Chem A Mater* **6**, 8109–8119 (2018).

6. Lu, Y., Guo, J., He, Z., Gao, Z. & Song, Y.-Y. Direct access to NiCo-LDH nanosheets by electrochemical-scanning-mediated hydrolysis for photothermally enhanced energy storage capacity. *Energy Storage Mater* **48**, 487–496 (2022).

7. Guo, Y. *et al.* Multicomponent hierarchical Cu-doped NiCo-LDH/CuO double arrays for ultralong-life hybrid fiber supercapacitor. *Adv Funct Mater* **29**, 1809004 (2019).

8. Zhai, Z. B., Huang, K. J. & Wu, X. Superior mixed Co-Cd selenide nanorods for high performance alkaline battery-supercapacitor hybrid energy storage. *Nano Energy* **47**, 89–95 (2018).

9. Kim, T. *et al.* Homogeneous Elongation of N-Doped CNTs over Nano-Fibrillated Hollow-Carbon-Nanofiber: Mass and Charge Balance in Asymmetric Supercapacitors Is No Longer Problematic. *Advanced Science* **9**, (2022).

10. Owusu, K. A. *et al.* Low-crystalline iron oxide hydroxide nanoparticle anode for high-performance supercapacitors. *Nat Commun* **8**, (2017).

11. Vaquero, S., Palma, J., Anderson, M. & Marcilla, R. *Mass-Balancing of Electrodes as a Strategy to Widen the Operating Voltage Window of Carbon/Carbon Supercapacitors in Neutral Aqueous Electrolytes*. *Int. J. Electrochem. Sci* vol. 8 www.electrochemsci.org (2013).

12. Krishnan, S. G. *et al.* Improving the symmetry of asymmetric supercapacitors using battery-type positive electrodes and activated carbon negative electrodes by mass and charge balance. *Journal of Electroanalytical Chemistry* **805**, 126–132 (2017).

13. Li, M., Cheng, J. P., Liu, F. & Zhang, X. B. 3D-architectured nickel–cobalt–manganese layered double hydroxide/reduced graphene oxide composite for high-performance supercapacitor. *Chem Phys Lett* **640**, 5–10 (2015).

14. Yu, C. *et al.* Nanohybrids from NiCoAl-LDH coupled with carbon for pseudocapacitors: understanding the role of nano-structured carbon. *Nanoscale* **6**, 3097–3104 (2014).

15. Zheng, X. *et al.* Construction of Ni-Co-Mn layered double hydroxide nanoflakes assembled hollow nanocages from bimetallic imidazolate frameworks for supercapacitors. *Mater Res Bull* **106**, 243–249 (2018).

16. Chen, T. *et al.* Three dimensional hierarchical porous nickel cobalt layered double hydroxides (LDHs) and nitrogen doped activated biocarbon composites for high-performance asymmetric supercapacitor. *J Alloys Compd* **859**, 158318 (2021).

17. Guan, X., Huang, M., Yang, L., Wang, G. & Guan, X. Facial design and synthesis of CoSx/Ni-Co LDH nanocages with rhombic dodecahedral structure for high-performance asymmetric supercapacitors. *Chemical Engineering Journal* **372**, 151–162 (2019).

18. Bai, X. *et al.* In-Situ Fabrication of MOF-Derived Co−Co Layered Double Hydroxide Hollow Nanocages/Graphene Composite: A Novel Electrode Material with Superior Electrochemical Performance. *Chemistry - A European Journal* **23**, 14839–14847 (2017).

19. Li, M., Ma, K. Y., Cheng, J. P., Lv, D. & Zhang, X. B. Nickel–cobalt hydroxide nanoflakes conformal coating on carbon nanotubes as a supercapacitive material with high-rate capability. *J Power Sources* **286**, 438–444 (2015).

20. Hou, C., Li, T., Zhang, Z., Chang, C. & An, L. Nickel-cobalt layered double hydroxide hollow nanocages anchored on carbon nanotubes as electrode for supercapacitors. *Mater Lett* **309**, 131361 (2022).

21. Tian, J. *et al.* Preparation of CoS2 supported flower-like NiFe layered double hydroxides nanospheres for high-performance supercapacitors. *J Colloid Interface Sci* **579**, 607–618 (2020).

22. Ma, K., Liu, F., Zhang, M., Zhang, X. & Cheng, J. P. Core/shell microrod arrays of NiO/Co-Fe layered double hydroxides deposited on nickel foam for energy storage and conversion. *Electrochim Acta* **225**, 425–434 (2017).

23. Sun, Q., Yao, K. & Zhang, Y. MnO2-directed synthesis of NiFe-LDH@FeOOH nanosheeet arrays for supercapacitor negative electrode. *Chinese Chemical Letters* **31**, 2343–2346 (2020).

24. Ni, C.-S. *et al.* Binder-free NiCoFe layered double hydroxide nanosheets for flexible energy storage devices with high-rate-retention characteristics. *Electrochim Acta* **384**, 138415 (2021).

25. Xiong, X. *et al.* Controlled synthesis of NiCo2S4 nanostructured arrays on carbon fiber paper for high-performance pseudocapacitors. *Nano Energy* **16**, 71–80 (2015).

26. Li, B. *et al.* Self-supporting graphene aerogel electrode intensified by NiCo2S4 nanoparticles for asymmetric supercapacitor. *Electrochim Acta* **314**, 32–39 (2019).

27. Huang, X. & Gou, L. High performance asymmetric supercapacitor based on hierarchical flower-like NiCo2S4@polyaniline. *Appl Surf Sci* **487**, 68–76 (2019).

28. Li, Y. *et al.* A NiCo2S4 /hierarchical porous carbon for high performance asymmetrical supercapacitor. *J Power Sources* **427**, 138–144 (2019).

29. Wang, G., Jin, Z. & Zhang, W. A phosphatized NiCo LDH 1D dendritic electrode for high energy asymmetric supercapacitors. *Dalton Transactions* **48**, 14853–14863 (2019).